JES Focus Issue on Advanced Techniques in Corrosion Science in Memory of Hugh Isaacs

Effect of Trace H_2S on the Scale Formation Behavior in a Predominant CO_2 Environment under Hydrodynamic Control: Role of Cr/Mo Micro-Alloying in Plain Carbon Steel

M. Hassan Sk,[1,2,a] J. Qi,[2,b] A. M. Abdullah,[1,*] N. Laycock,[3] M. P. Ryan,[2] and D. E. Williams[4,z]

[1] *Center for Advanced Materials, CAM, Qatar University, Doha, 2713, Qatar*
[2] *Department of Materials, Imperial College London, SW7 2AZ, United Kingdom*
[3] *Qatar Shell Research & Technology Centre, Doha, Qatar*
[4] *MacDiarmid Institute for Advanced Materials and Nanotechnology, School of Chemical Sciences, University of Auckland, Auckland 1042, New Zealand*

The effects of the presence of trace H_2S (~ 0.5 μM total dissolved H_2S) on the electrocrystallization of siderite on plain carbon steel and its various micro-alloyed counterparts are explored. This small concentration of H_2S in a CO_2 saturated (sweet) brine (0.5 M NaCl), at 80°C, in a slightly acidic environment (pH 6.6) at the elevated temperature was found to increase the anodic dissolution rate of the plain carbon steel and inhibit the electrocrystallization of carbonate scale. Highly porous surface scales resulted that contained sulfide uniformly distributed through the thickness through which anodic dissolution of the steel proceeded. There was a strong dependence on both electrode rotation rate and on micro-alloying (Cr, Mo) of the scale formation kinetics, morphology and eventual scale protectiveness. For the 1Cr steel, the electrocrystallization of carbonate was inhibited but was still observable electrochemically. The resultant scale was highly porous but contained little sulfur. With sufficient Mo (0.7 wt%) in the 1Cr steel, a two-layer scale was formed, with the inner layer coherent but not containing appreciable sulfur: it was probably a carbonate. With sufficient Cr (3.5 wt%) a coherent and protective layer, presumed to be a chromium oxide or oxyhydroxide that also contained Fe, 200–600 nm thick, protected the steel from the anodic activation by H_2S. The results contrast with literature results for similar H_2S concentrations at room temperature or for higher concentrations at elevated temperature, where passivating films of iron sulfide have been reported. The effect of trace H_2S on the formation of protective, crystalline siderite scales at elevated temperature is a possible mechanism for initiation of corrosion of pipeline steels in operational conditions in nominally 'sweet' fields.

 [DOI: 10.1149/2.0311911jes]

Manuscript submitted March 28, 2019; revised manuscript received May 9, 2019. Published May 16, 2019. *This paper is part of the JES Focus Issue on Advanced Techniques in Corrosion Science in Memory of Hugh Isaacs.*

Internal corrosion of carbon steel pipelines in CO_2/H_2S environments and the effects of alloy composition on this have been investigated over the last six decades.[1–11] In a mixed CO_2-H_2S environment, the corrosion phenomena are more complex than in the single-gas counterparts: a simple additive measure of the individual effects of H_2S and CO_2 does not represent the effect observed in a combined CO_2-H_2S environment.[1,4] In a combined CO_2-H_2S environment, low concentrations of H_2S can either promote anodic dissolution, promote localized corrosion, or may decrease corrosion.[6–12]

The CO_2/H_2S environment is generally divided into three categories on the basis of the partial pressure ratio of these two acidic gases (i.e. pCO_2: pH_2S) as introduced by Pots et al.[13] When pCO_2: $pH_2S \geq 500$, the environment is essentially recognized as 'sweet' where the effect of H_2S is considered small. This scenario has been of special interest and a number of studies[5,6,10,14–17] have demonstrated that within the sweet regime, even the presence of a trace amount of H_2S can bring a significant change in the nature of any corrosion scale and its protectiveness. Many studies,[5,6,10,14,15,18–24] principally conducted at room temperature and with H_2S aqueous concentrations in the range 0.3 – 50 μM, have indicated the formation of mackinawite as a primary corrosion product in the form of an extremely thin film, causing an immediate reduction in the corrosion rate for the case of plain carbon steel (mild steel). To make comparisons, we have converted gas phase mixing ratios and partial pressures to solution concentration using Henry's law constant, dissociation constant of H_2S and the temperature[25] and salt concentration dependence.[26] For example, Choi et al.[5] studied the effects of a small amount of H_2S (100 ppm, 0.01 kPa H_2S in 0.1MPa CO_2, i.e. ~ 10 μM) at RT, pH 3–4, 1 wt% brine, 1000 RPM on 1018 plain carbon steel. With the incorporation of this small level of H_2S into the gas, they found that the corrosion rate dropped to 0.25 mm/yr (for both pH 3 and 4) from 4mm/yr. (at pH 3) and 1.75 mm/yr (at pH 4) observed under the CO_2 – only condition. With the removal of the trace level of H_2S from the gas, the corrosion rate increased. No significant change in the surface morphology was detected in the presence or absence of trace H_2S. Energy dispersive X-ray analysis in the scanning electron microscope detected only Fe and C at the steel surface. X-ray photoelectron spectroscopy, however confirmed the presence of sulfide as well as carbonate in coexistence on the surface.

Smith and Pacheco[16,17] specifically considered the problem of corrosion in 'slightly sour' environments, work recently extended to explore the problem of localized corrosion in such environments.[6,10] Smith and Pacheco defined sour corrosion as a series of corrosion mechanisms that are defined by the formation of a type of iron sulfide, and slightly sour corrosion is that regime where the corrosion product is mackinawite. Their review of the literature indicated that mackinawite is a thermodynamically semi-stable form of ferrous sulfide that forms on the steel surface under conditions where iron sulfide is still soluble in the bulk solution; i.e., the concentrations of Fe^{2+} and H_2S are still below the saturation point of the bulk solution. By consideration of the thermodynamics, they defined a critical H_2S concentration for transition between carbonate-controlled corrosion and mackinawite-controlled corrosion. They also noted that the consumption of Fe^{2+} by sulfide formation keeps the Fe^{2+}(aq) concentration low and thereby retards $FeCO_3$ precipitation. Their measurements at 50°C showed a significant drop in corrosion rate of carbon steel for concentrations of H_2S in the solution somewhere in the range 34 – 167 μM. Over the 3-day test, corrosion rates determined by weight loss were ~ 4 mm/yr in the lower range of H_2S concentration and

*Electrochemical Society Member.
[a]Present address: BP Institute and Department of Chemistry, Cambridge University, Cambridge CB2 1EW, United Kingdom.
[b]Present address: Department of Materials Science and Engineering, The University of Sheffield, S1 3JD, United Kingdom.
[z]E-mail: david.williams@auckland.ac.nz

~2 mm/yr in the higher range. Sun and Nesic[18,24] reported somewhat lower corrosion rates: at 50°C, pH 6.6, 700 μM H_2S, of 2 mm/yr over 1 hr reducing to 0.3 mm/yr over 24 hr; and at 80°C, 50 μM H_2S, of 2 mm/yr over 1 hr reducing to 0.2mm/yr over 24 hr. Esmaeely et al.[6] and Zhang et al.[10] noted that the presence of trace H_2S in CO_2 caused localized corrosion, particularly at lower temperature (30°C but not at 60°C or greater) pH (<6) and H_2S concentration (0.8 – 4 μM). The latter authors noted the importance of the microstructure of the steel, inferring that supersaturation within a matrix of Fe_3C left after corrosion provided the condition for protective scale formation - an effect that has also been deduced as important for the formation of crystalline siderite ($FeCO_3$) scales.[27,28]

There have been few studies of the effects of low-alloy additions on corrosion behavior in 'slightly sour' environments. Kermani et al.[2] reported the development of superior corrosion resistance 3% Cr steels for downhole applications. Liu et al.[29] provided a qualitative demonstration of steel with 3 wt% Cr in CO_2-H_2S environment where they indicated the performance of this steel to be superior compared to ordinary plain carbon steel. Laycock[30] observed the effects of micro-alloying (< 2 wt%) with Cr, Mo on the corrosion behavior of carbon steel in 1M aqueous NaCl saturated with H_2S at 1 atm and identified a strong pH dependence.

In our previous work,[27,28,31–37] we showed that the formation of carbonate scales at elevated temperature in CO_2-saturated brine was a complex process: the steel undergoes anodic dissolution (assumed as a carbonato-complex); colloidal material is precipitated in the solution; siderite and chukanovite scales are formed on the metal surface by electrocrystallization. A high critical supersaturation is required for crystal nucleation leading to important effects of electrode potential, flow and local environment determined by the microstructure developed during anodic dissolution. The critical supersaturation is sensitive to the presence of traces of high-valent metal ions in solution, leading to important effects of micro-alloying on the formation of protective scales. The surface pH also seemed to play an important role in determining the balance between siderite and chukanovite, and thus the morphology of the surface scale. The whole system is thus sensitive to hydrodynamics and to transport within the surface roughness developed as a consequence of the dissolution.[27] As noted by Smith and Pacheco,[16,17] dissolved H_2S would have a significant effect on the supersaturation for crystallization of ferrous carbonates, and at low concentration the effect would be dependent on the transport rate of sulfide to the interface. Our earlier works in pure CO_2 brine solutions indicated as an important effect a decrease in the critical supersaturation and enhancement of the crystallization rate of siderite in the presence of Cr^{3+}.[33,35] Our recent investigations[37,38] suggested that there exists a synergistic interaction between Cr and Mo, which induces more rapid crystallization of the scale compared to Mo-free steels. We suggested[37] an interaction between Cr and Mo in a standalone CO_2 environment, leading to the idea that an optimized addition of Mo might replace a much higher percentage of Cr for a similar degree of corrosion protection. From a mechanistic perspective, we suggested that the addition of small amounts of Cr/Mo modulates the current due to dissolution of iron, as well as the current due to growth of a crystalline layer. We further suggested that Cr/Mo species in solution at the metal interface significantly accelerate electrocrystallization of siderite. Based on our previous findings,[33] and on other evidence[39,40] in the literature we suggested that the formation of the crystalline scale is a form of particle-mediated or aggregation-based growth of crystals and as such very sensitive to adsorption of other species on the initial amorphous phase. We hypothesized that substitution of ions of micro-alloy components into Fe^{2+} sites at the surface of nano-scale clusters of amorphous iron carbonate might alter the surface charge and perhaps thereby alter the kinetic barrier to crystallization. However, in the presence of trace H_2S, dissolution of micro-alloy components (e.g. Cr) would lead to the precipitation of their very insoluble sulfides in the solution, as would the dissolution of Fe. Thus, given some rate of anodic dissolution, there should be a transport-determined process, of H_2S from the solution into a reaction zone near the corroding surface, which will be dependent on the precipitation rate of sulfide colloid and of carbonate colloid and which will in turn determine the sulfide concentration at the metal surface and the composition and perhaps the corrosion protection efficacy of any scale that is formed. There might also be an effect of any sulfide in solution or sulfide colloid on the crystallization of the carbonates. Alloy composition- and hydrodynamic-dependent complexity in the electrochemical behavior of steels in the presence of traces of H_2S in CO_2 at elevated temperature is therefore to be anticipated.

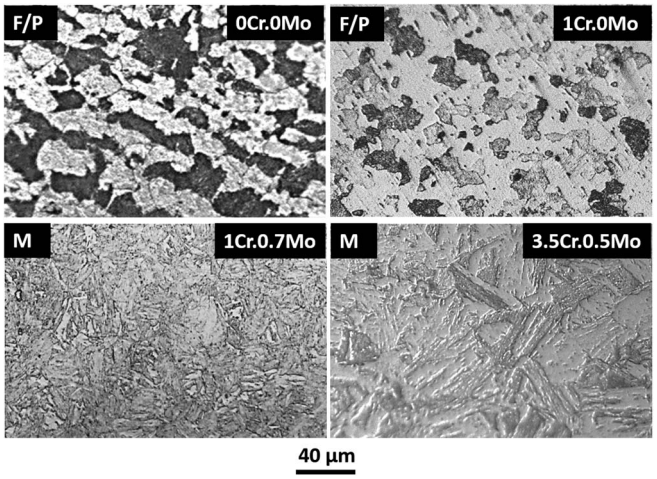

Figure 1. Metallographic microstructures of the 4 steels. Polished to 0.3 μm with alumina; 3% Nital etched. F/P: Ferritic/ Pearlitic; M: martensitic.

In the present work we use four different steels, including the plain carbon steel and its Cr, Mo micro-alloyed counterparts. The dependence on micro-alloying (Cr, Mo) and flow velocity, of the scale formation and eventual scale protectiveness in the presence of trace H_2S in a predominantly (CO_2 saturated) sweet regime has been studied by constructing a novel experimental set-up and protocol, that addresses safety concerns associated with the use of H_2S; whilst allowing conventional RDE experiments to be performed.

Materials and Methods

Materials.—A number of different steel samples were used in this study: API J55 plain carbon steel and 1Cr (E47), 1Cr.0.7Mo, and 3.5Cr.0.5Mo.0.2Cu low alloy steels. The chemical compositions are shown in Table I. The microstructure changes from ferritic/pearlitic to martensitic with increasing extent of micro-alloying (see Figure 1). Samples were machined from a pipeline sample to produce round bars of diameter 6 mm which were then customized to be used as rotating-disk working electrodes (RDE). The samples were cut to 15 mm length pieces which were then inner-threaded from one end, ultrasonically cleaned with n-butane for 10 min, washed with distilled water and dried. The samples were then mounted using epoxy resin into a poly tetra fluoro ethylene (PTFE) shield[25] and the exposed surface was ground to a 15 μm surface finish using silicon carbide paper.

Test solution.—The base test solution for all experiments was 0.5 M NaCl. The electrolyte was purged with high-purity CO_2 (supplier specification < 2ppm O_2) until the pH was stable (pH ~ 3.9; approx. 30 min). Then the solution was adjusted to pH 6.3 at room temperature (at 80°C calculated pH 6.6[28]) by addition of 2 M NaOH then the temperature was increased to 80°C with CO_2 continuously bubbling through the solution. For experiments with H_2S, this gas was then dosed at low concentration into a CO_2 stream to obtain a particular dissolved concentration. H_2S was chemically generated in a separate flask by injecting dilute HCl (2M) at 0.2 mL min^{-1} into an aqueous Na_2S solution, rapidly stirred under a flowing CO_2 atmosphere. The gas flow into the electrochemical cell was switched from CO_2 –only to the H_2S-CO_2 stream for a defined time, then switched back to CO_2 –

Table I. Bulk Composition (wt%) of the Alloys: (Certified chemical analysis provided by the supplier)

Steel samples	Composition: wt% (and Fe bal.)										
Grades	C	Si	Mn	Cr	Mo	S	P	Ni	Cu	Al	V
0Cr.0Mo	0.29	0.33	1.30	0.06	0.04	0.001	0.009	0.02	0.02	-	0.001
1Cr. 0Mo	0.52	0.38	0.67	0.94	-	0.025	0.033	-	-	-	0.165
1Cr.0.7Mo	0.28	0.23	0.30	1.05	0.7	0.001	0.008	0.03	0.06	-	0.045
3.5Cr.0.5Mo	0.08	0.31	0.54	3.51	0.51	0.001	0.01	0.05	0.21	-	0.14

only, thus dosing a fixed amount of H_2S into the solution. The working and reference electrodes were inserted into this solution and the electrode rotation started. A double junction Ag-AgCl /sat. KCl reference electrode was used and was mounted externally and connected to the cell via a Luggin capillary containing the NaCl solution. The working electrode was polarized to -1 V Ag/AgCl for 2 minutes to cathodically reduce any air-formed film then returned to open-circuit until the corrosion potential, E_{corr}, stabilized ($\sim$ 2 min); then the potential was stepped to E_{corr} + 150 mV (an electrode potential at which previous work had shown the electrocrystallization transient to be easily observable[28,37]) and the current transient recorded. CO_2 was purged at 30 mL.min^{-1} throughout the procedure. The experimental arrangement is shown in Figure 2.

Hydrogen sulfide concentration in the gas was determined using a simple colorimetric flow tube (Gastec type 4L, Gastec Corporation, Japan) connected in the outlet from the cell. Solid lead acetate reacts with H_2S; an advancing front of brown PbS shows the total amount of H_2S within a fixed volume of gas passing through the tube. The tube scale is calibrated for a total gas volume of 100 mL. With the electrochemical cell empty, we measured the concentration value indicated on the scale as a function of time after starting the injection of HCl into the generator flask (Figure 2b). After a delay ascribable to the time needed to stabilize the reaction rate in the mixing flask and fill the flow lines and electrochemical cell with the H_2S-CO_2 mixture, the indicated scale concentration increased linearly with time. From the slope of this line, the flow rate and the standard volume for the tube we calculate the concentration of H_2S in the gas stream as 19 ppmv (parts per million by volume). With NaCl solution in the electrochemical cell, the gas detector tube did not detect H_2S in the exit gas. Hence all of the H_2S dosed into the cell remained in solution, within the limits of detection of this apparatus. The dosing time was 21 min, meaning that the total H_2S concentration in the solution was 0.5 μM before the electrodes were assembled into the cell. Some H_2S would have been lost during this procedure and into the gas stream

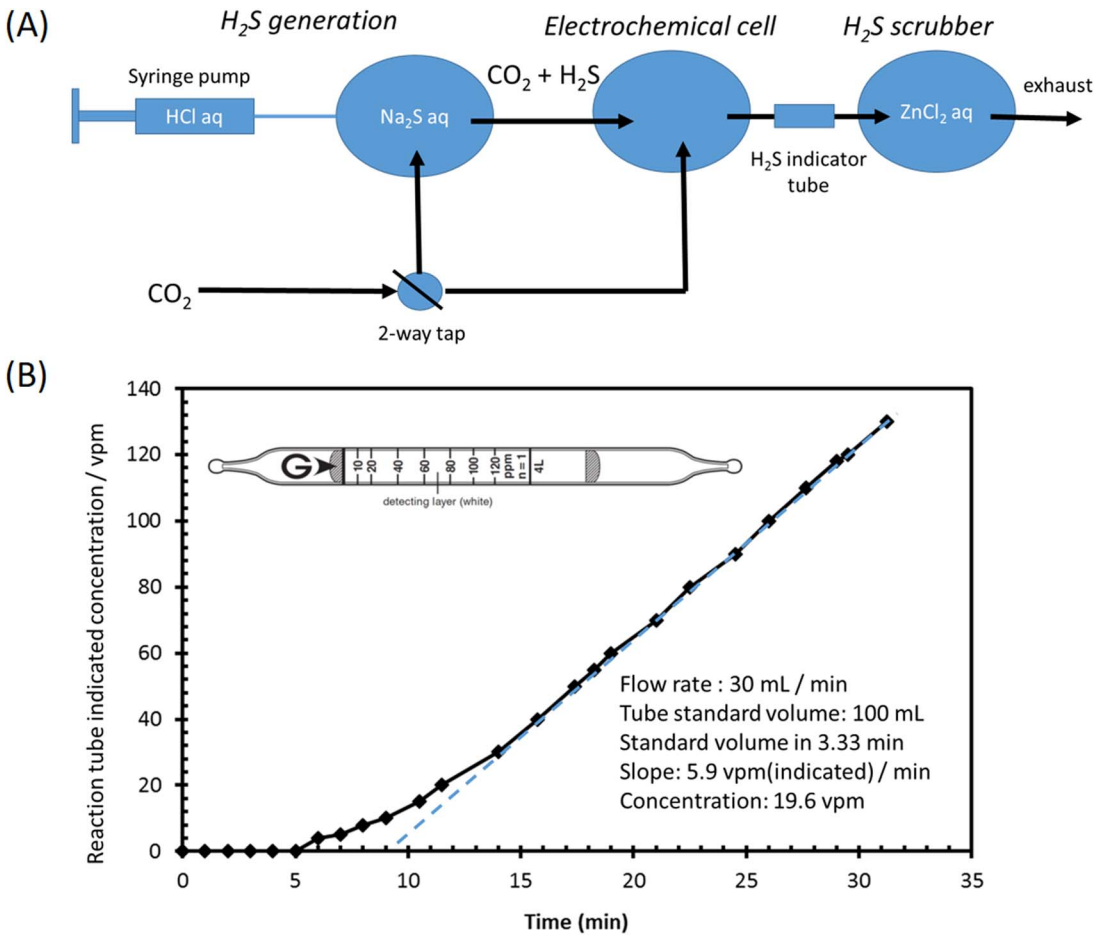

Figure 2. (A) Schematic of the experimental arrangement. Gaseous H_2S generated via chemical route is driven by CO_2 gas and carried through the inlet of the experimental cell, the outlet of which connected to the double fold H_2S trap. (B) Variation of H_2S concentration at the outlet of the electrochemical cell, in the absence of electrolyte, determined using the progression of the indicator color in a simple colorimetric flow tube, from which the concentration of H_2S in the gas stream is estimated.

during the electrochemical measurement, hence the stated concentration is an upper limit. Since the detector tube mounted in the exit from the electrochemical cell detected no H_2S during the duration of the measurement, we have assumed that any loss was small.

The first dissociation constant of H_2S has been given as $10^{-2.5}$ mol dm^{-3};[41] hence at pH 6.6, $HS^-$is the dominant species. The initial precipitation product is an amorphous iron sulfide for which the solubility product is $[Fe^{2+}][HS^-]/[H^+] \approx 10^{-3}$.[42] The solubility product for crystalline forms, obtained by ageing the precipitate in the solution, is smaller;[8] the solubility product increases with increasing temperature.[43] Under the solution conditions used here, therefore, precipitation of ferrous sulfide would require concentrations of Fe^{2+} on the mM scale. Hence the experiment probes a very particular case of very small H_2S concentration, close to or below the limit for precipitation of ferrous sulfide near the electrode surface. The experiment is in the 'slightly sour' regime defined by Smith and Patcheco,[16,17] and specifically in the range noted by them where the corrosion rate is high, not that where a mackinawite film is supposed to limit the dissolution rate. The experiment thus explores the effect of traces of H_2S on the carbonate-controlled corrosion. Furthermore, since the experiment probes the effect of anodic polarization with measurement of the resulting current over a time of 15 – 25 min (see Figure 3) it particularly addresses the effect of traces of H_2S on the electrocrystallization of the surface carbonate. Although the experiment does not address measurement of corrosion rates at open-circuit over long time scales (these have been well-explored by others as noted above), it does address basic phenomena of importance to understanding the evolution of the corrosion scales that are known to control behavior in the long term.

The electrochemical tests were carried out in a 1 L double jacketed glass cell. Water was circulated through the outer jacket of the cell at a constant temperature. The experiments were controlled using a

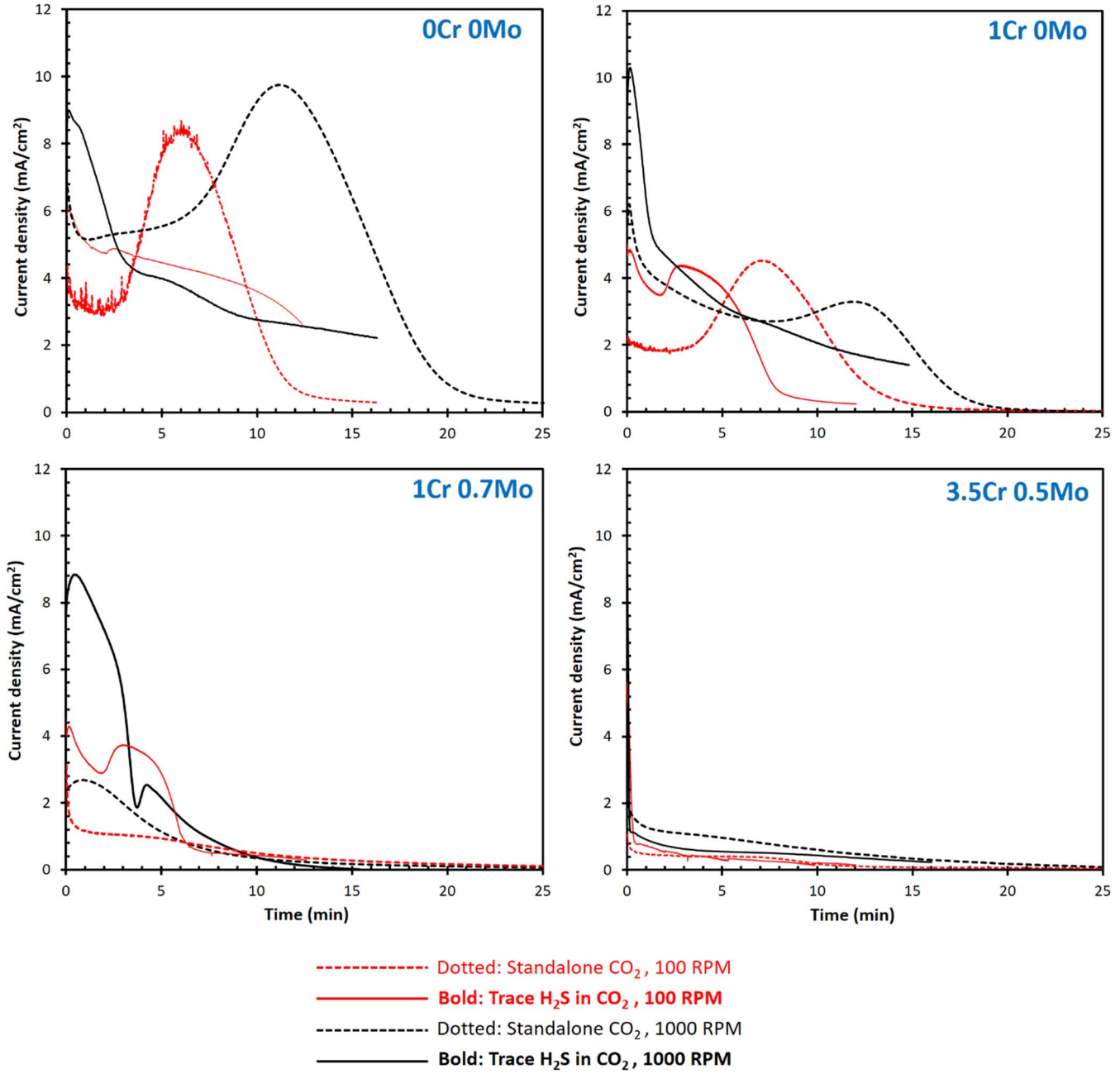

Figure 3. Comparison of the potentiostatic current transients on the different steels following the step from E_{corr} to E_{corr} + 150 mV; 'standalone' CO_2 and in the presence of trace H_2S (0.5 μmol dm^{-3}) at 100 and 1000 RPM. Electrolyte: 0.5 mol dm^{-3} aqueous NaCl, pH 6.6 at 80°C.

Table II. Corrosion potentials measured at 80°C with respect to an external reference electrode, for the different steels and conditions.

E_{corr} (Ag/AgCl)	J55 carbon steel	1Cr	1Cr0.7Mo	3.5Cr0.5Mo
CO_2 - *only*	−730 ± 10 mV	−720 ± 15 mV	−715 ± 10 mV	−710 ± 10 mV
CO_2 – *trace* H_2S	−760 ± 10 mV	−745 ± 10 mV	−740 ± 10mV	−730 ± 15 mV

Gamry 600 potentiostat. The counter electrode (CE) was a Pt wire ring in the plane of, and centered on the working electrode (WE). As noted above, the Ag,AgCl / sat KCl reference electrode was held externally and connected to the cell via Luggin capillary containing the test solution; the tip of the capillary was centered on the WE. The RDE was controlled using a Gamry RDE710 Rotating Electrode regulator. At the end of each run, the electrode was removed into the air, washed, dried, detached from the rotating disc assembly and stored in a desiccator in air. The electrodes were examined using X-ray diffractometry (XRD), and cross-sections were prepared using a focused ion beam (FIB: Helios NanoLab 600 from FEI) and analyzed in a transmission electron microscope (TEM: JEOL-2100F).

Results and Discussion

Figure 3 shows the very significant alloy- and flow-dependent effect of trace H_2S on potentiostatic current transients in a CO_2 saturated environment. Table II shows the corrosion potential at the start of each measurement.

For all the alloys except the 3.5Cr steel, the effect of trace H_2S was to significantly increase the initial anodic current density. The increase in anodic dissolution rate is consistent with the decrease of corrosion potential at the start of the experiment. On the plain carbon steel, the peak due to nucleation and growth of the carbonate,[28] seen in the absence of H_2S, disappeared in the presence of trace H_2S. On the micro-alloyed steels with 1Cr, at low rotation rate a peak was observed, but it was very broad. At high rotation rate, the initial activation of the steel seemed greater. These effects are difficult to interpret in detail. However, although the current decreased in the presence of trace H_2S, certainly as a consequence of the presence of the trace of H_2S, the electrocrystallization of a protective surface scale was significantly affected. There was an activation of the dissolution at short times, and the formation of any coherent and protective layer, such as a carbonate, seemed significantly inhibited for plain C steel at 100 RPM and for both C-steel and 1%Cr at 1000 RPM.

X-ray diffraction (XRD) (Figure 4), measured ex-situ after washing and drying, was inconclusive since the surface layers formed in these experiments were rather thin, though it indicated that siderite, formed in the pure CO_2 environment, was not found after the experiments in the presence of trace H_2S. Instead, chukanovite was indicated, together with mackinawite

Examination of cross-sections of samples following anodic dissolution, made using focussed-ion beam-sectioning, showed that the morphology of the scale was very sensitive to microalloying and reinforced the deduction from the electrochemical behavior. The observed morphology was very different on the different alloys though one common characteristic was a highly porous layer of material that could cover a more coherent layer, depending on the alloy composition. On the plain carbon steel, Figure 5, scales were 2 – 4 μm thick with a highly porous microstructure. Sulfur was distributed throughout the scale. No thin adherent sub-film next to the metal surface was detected. In the absence of microalloying, the scale appeared to be a mixed sulfide-carbonate (based on the detection of oxygen in the scale). There was no evidence of a coherent, crystalline scale such as was formed in the absence of trace H_2S.

For the 1Cr steel (Figure 6), sulfur was detected on the outside of the scale, which again appeared to be a carbonate, with a sulfide above. For the 1Cr0.7Mo steel (Figure 7), there was a coherent layer ~ 1 μm thick next to the metal surface. This layer appeared to contain dominantly iron and is assumed to be $FeCO_3$. Above was a highly porous layer that was ~3 μm thick, that contained both Cr and Fe. There were only traces of sulfur in this layer.

For the 3.5Cr steel (Figure 8), the metal surface was covered by a 200–600 nm thick, coherent layer, that contained Fe but also showed a strong signal for Cr, significantly above the level for the metal. This layer also showed a strong oxygen signal. A reasonable assumption is that it was a chromium oxide or oxyhydroxide containing some iron perhaps as a spinel. This observation of an inner Cr-rich layer is consistent with others.[29,44–46] Sulfur was found in a thicker layer also containing Fe that was above this.

In our previous work[28,37] we demonstrated that the potentiostatic current transients in the CO_2 environment follow a general pattern for both plain carbon steel as well as Cr/Mo micro-alloyed steels. There are two current components: a current due to dissolution which falls

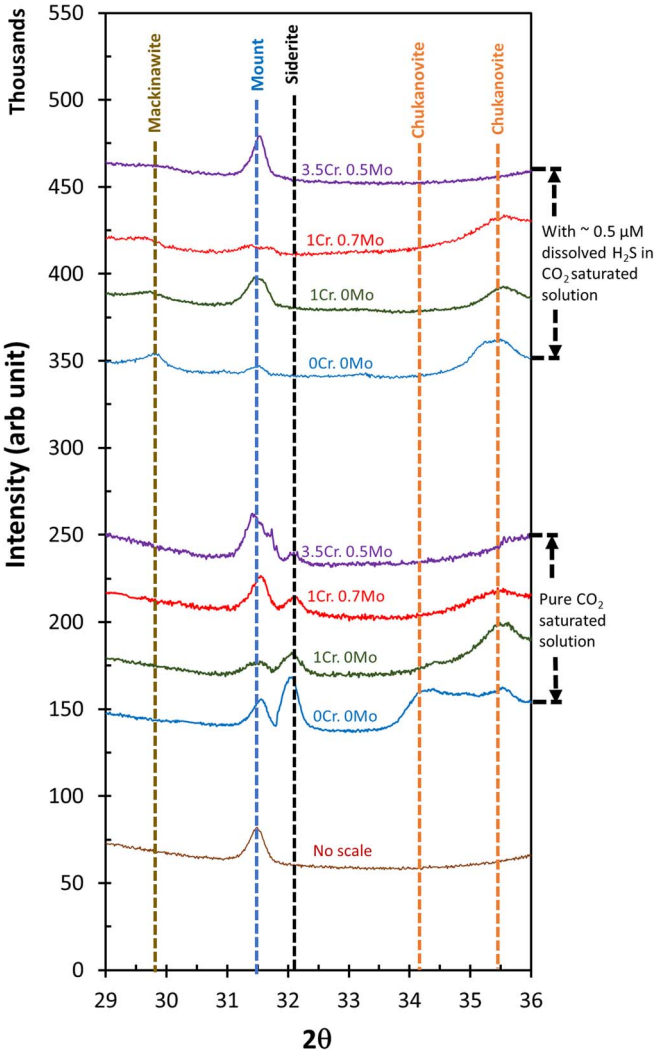

Figure 4. Ex-situ XRD patterns (overnight scan) of corrosion scales formed on plain carbon and Cr-Mo micro-alloyed steels in absence and presence of trace (~0.5 μM) H_2S in a CO_2 saturated hot brine environment. 'No scale' is the pattern from the polished iron specimen. potential = E_{OC} + 150 mV, pH = 6.6, Temp = 80°C, in 0.5 M NaCl. Wavelength: Cu Kα, λ = 1.54 Å.

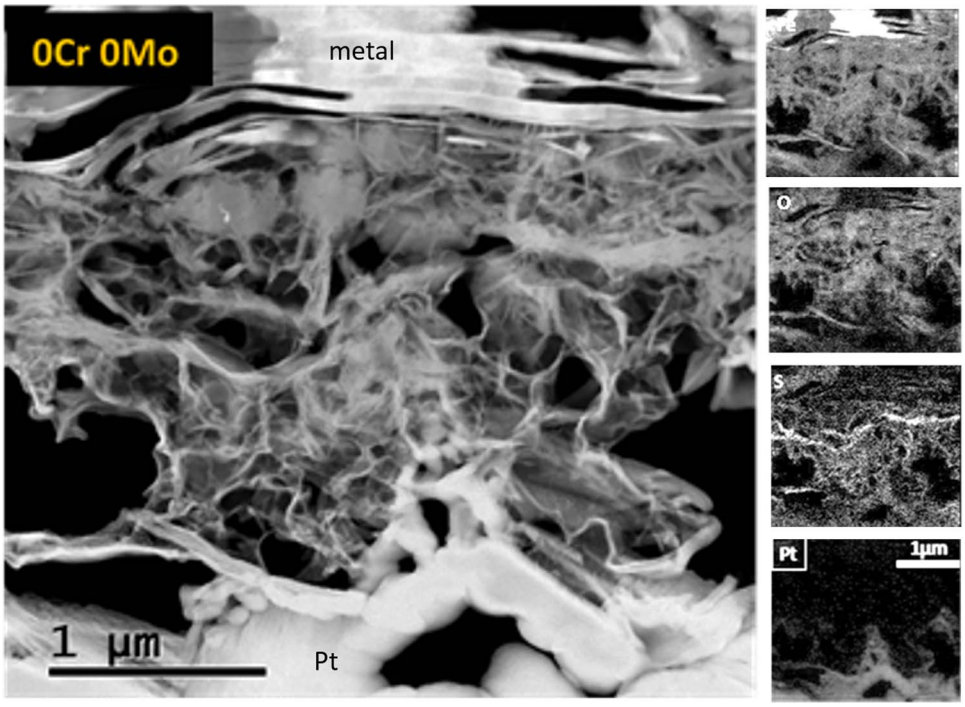

Figure 5. FIB-cross section of the scale formed on plain carbon steel (J55) in the presence of trace H_2S (0.5 µmol dm^{-3}) at 1000 RPM. Electrolyte: 0.5 mol dm^{-3} aqueous NaCl, pH 6.6 at 80°C. Pt is deposited on the outside of the scale to support the cross-section. The X-ray maps (right) have been brightness and contrast enhanced to show clearly the location of the different elemental species and are indicative of relative concentration only within each image.

rapidly to a plateau following the anodic potential step; and a current due to electrocrystallization, which rises through a peak before decaying to a low value as the crystalline layer spreads over the surface. In Figure 3 these transients are shown for the various steels. The effect of the addition of H_2S depended on the alloy and the electrode rotation rate. However, in general it was a suppression of the electrocrystallization peak, its broadening and its initiation moving to shorter time following the anodic potential step. There were differences in detail,

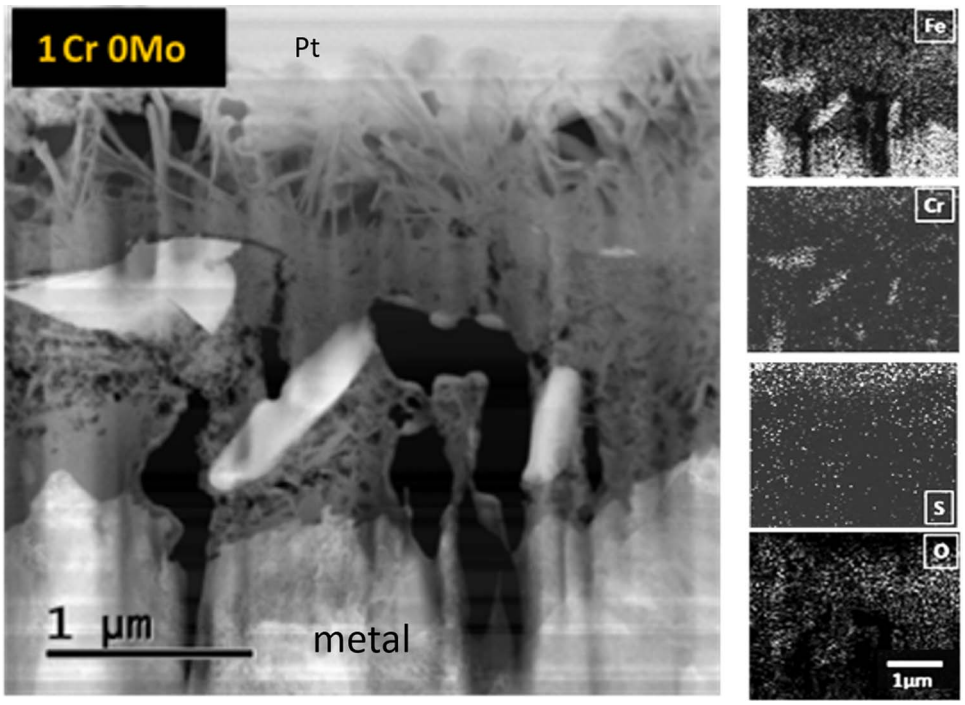

Figure 6. FIB-cross section of the scale formed on 1Cr steel in the presence of trace H_2S (0.5 µmol dm^{-3}) at 1000 RPM. Electrolyte: 0.5 mol dm^{-3} aqueous NaCl, pH 6.6 at 80°C. Pt is deposited on the outside of the scale to support the cross-section. Fragments of metal have been detached from the surface and incorporated into the scale, which is deduced to be a carbonate with a sulfide layer on top. The X-ray maps (right) have been brightness and contrast enhanced to show clearly the location of the different elemental species and are indicative of relative concentration only within each image.

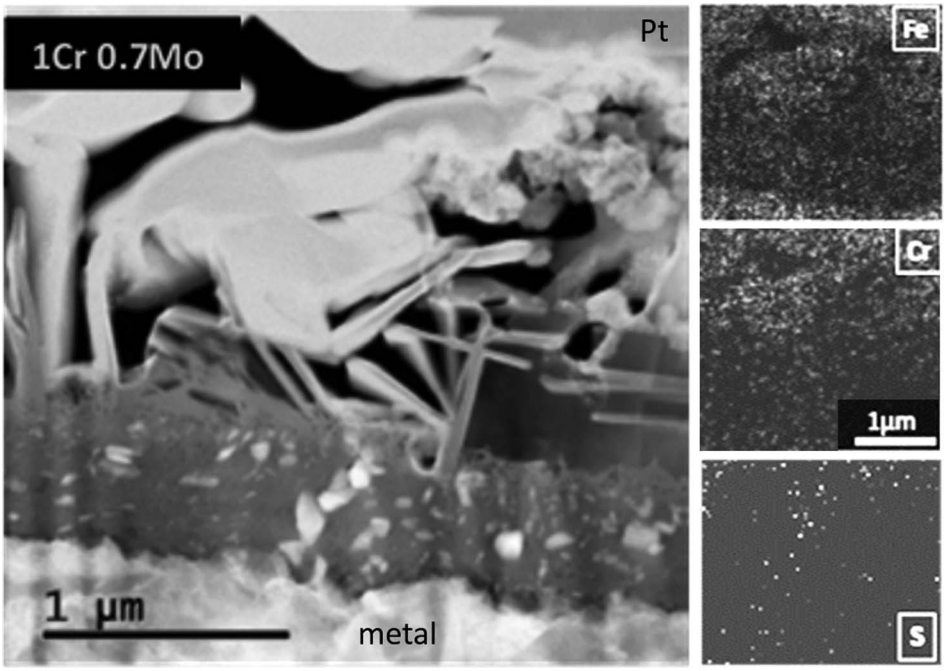

Figure 7. FIB-cross section of the scale formed on 1Cr 0.7Mo steel in the presence of trace H_2S (0.5 µmol dm^{-3}) at 1000 RPM. Electrolyte: 0.5 mol dm^{-3} aqueous NaCl, pH 6.6 at 80°C. Pt is deposited on the outside of the scale to protect the sample during FIB process and to support the cross-section. The X-ray maps (right) have been brightness and contrast enhanced to show clearly the location of the different elemental species and are indicative of relative concentration only within each image. The Mo signal was not distinguishable from noise.

that depended on the alloy and the rotation rate. The initial current following the anodic potential step was higher in the presence of H_2S. This increase of current was notable for the steels containing Mo. At high rotation rate, the electrocrystallization peak tended to be less pronounced: the current tended to decay monotonically. For the 3.5Cr steel, the current was much lower than for the other steels and decayed rapidly to low values, explicable by the formation of the 200–600 nm thick, coherent, high-Cr layer, observed in the micrographs.

Rather than passivating the steel, at the low concentrations used in the present work H_2S initially enhanced the dissolution rate. There was no evidence of coherent surface layers forming for the C-steel or the 1%Cr steel, or for sulphide-containing layers on any of the steels: sulfur was generally only seen on the outside of the layer or within porous layers, consistent with precipitation of ferrous sulfide from solution. As a consequence of an enhanced dissolution rate of iron, the supersaturation for carbonate would be increased so the crystallization of carbonate would be accelerated. The resultant sulfide colloid may also affect nucleation of carbonate scale. However, the effect of transport in the system is complicated, since transport of HS^- and its reaction with iron dissolved from the metal must also be considered.

In our earlier work, we had noted the beneficial effect of a higher Mo concentration on the behavior of 1Cr-Mo steels in the CO_2-only environment.[37] In the present work, it is seen that this beneficial effect extends to an acceleration of passivation in an environment containing trace H_2S. The effect seems significantly larger than those effects due simply to change of microstructure previously reported.[27] The micrographs indeed show that the scale on the 1Cr0.7Mo alloys displays a coherent inner layer that is neither a sulfide nor a chromium oxide,

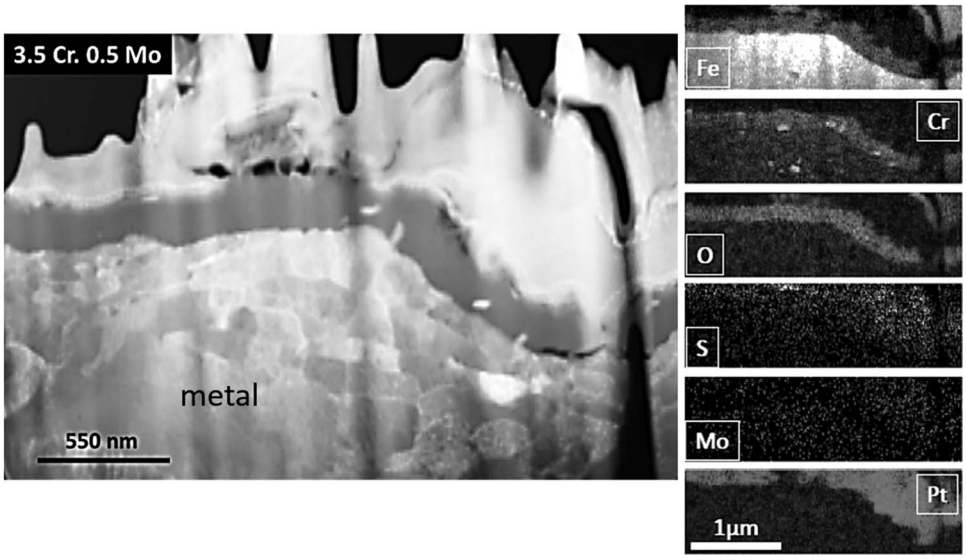

Figure 8. FIB-cross section of the scale formed on 3.5Cr 0.5Mo steel in the presence of trace H_2S (0.5 µmol dm^{-3}) at 1000 RPM. Electrolyte: 0.5 mol dm^{-3} aqueous NaCl, pH 6.6 at 80°C. Pt is deposited on the outside of the scale to protect the sample during FIB process and to support the cross-section. The X-ray maps (right) have been brightness and contrast enhanced to show clearly the location of the different elemental species and are indicative of relative concentration only within each image.

consistent with the ideas advanced previously on the synergistic effect of Cr and Mo on the formation of a protective carbonate.[37]

A tantalizing possibility that arises from consideration of the results of the present work concerns the effect of very small concentrations of H_2S on the initiation of corrosion attack in hot, CO_2-saturated brine. Very low H_2S concentrations have been shown here to *activate* the dissolution of carbon steel, promote the formation of highly porous scales and thus significantly to inhibit the formation of a protective crystalline carbonate scale. These effects have also been deduced to be very sensitive to local transport conditions. It is therefore conceivable that the presence of traces of H_2S, not unreasonable to suppose in production wells, could indeed lead to enhanced dissolution in localized areas. Furthermore, small increases in small H_2S concentrations might explain industry experience in which repair of a section of pipe which over time had become well-protected by a carbonate scale could lead to an unexpectedly high corrosion rate of the new section. Based on the present work, a speculative interpretation would be that the increased H_2S inhibits the formation of protective carbonate on the new surface.

Conclusions

A small concentration of H2S was found to activate the dissolution of the plain carbon steel, inhibit the electrocrystallization of carbonate and induce highly porous surface scales which could not prevent further anodic dissolution. The scale contained uniformly distributed sulfide through the thickness.

A strong dependence on flow velocity and micro-alloying (Cr, Mo) has been observed, of the scale formation kinetics, morphology and eventual scale protectiveness in the presence of trace H_2S in a predominantly (CO_2 saturated) sweet regime.

For the 1Cr steel, a highly porous scale containing a small amount of sulfur was found. With increasing Mo (0.7 wt%) in the 1Cr steel, a two-layered scale was observed where the inner layer is presumed to be a coherent carbonate layer with no appreciable sulfur. With increasing Cr content (3.5Cr), a more coherent and protective, 200–600 nm thick layer, presumably of chromium oxide or oxyhydroxide also containing Fe, was observed which prevented anodic activation of the steel by H_2S.

We speculate that the anodic activation by trace H_2S and inhibition of electrocrystallization of protective siderite scales is a possible mechanism for initiation of corrosion of pipeline steels in operational conditions in nominally 'sweet' fields.

Acknowledgment

MPR currently holds a Royal Academy of Engineering/Shell Research Chair. DEW acknowledges support from the MacDiarmid Institute for Advanced Materials and Nanotechnology, NZ. This work was supported by the Qatar National Research Fund, contract NPRP 7 - 146 - 2 – 072.

ORCID

A. M. Abdullah https://orcid.org/0000-0001-8406-9782
M. P. Ryan https://orcid.org/0000-0001-8582-3003
D. E. Williams https://orcid.org/0000-0003-4123-5626

References

1. S. N. Smith and M. W. Joosten, in *Corrosion 2006*, p. paper 6115 (2006).
2. B. Kermani, J. C. Gonzales, G. L. Turconi, L. Scoppio, G. Dicken, and D. Edmonds, in *Corrosion 2003*, p. paper 3116 (2003).
3. B. Kermani, J. W. Martin, and K. A. Esaklul, in *Corrosion 2006*, p. paper 6121 (2006).
4. M. Kermani and A. Morshed, *Corrosion*, **59**, 659 (2003).
5. Y.-S. Choi, S. Nesic, and S. Ling, *Electrochimica Acta*, **56**, 1752 (2011).
6. S. N. Esmaeely, W. Zhang, B. Brown, M. Singer, and S. Nesic, *Corrosion*, **73**, 1098 (2017).
7. J. Ning, Y. Zheng, B. Brown, D. Young, and S. Nesic, *Corrosion*, **73**, 155 (2017).
8. J. Ning, Y. Zheng, D. Young, B. Brown, and S. Nešić, *Corrosion*, **70**, 375 (2013).
9. F. Pessu, R. Barker, and A. Neville, *Corrosion*, **73**, 1168 (2017).
10. W. Zhang, B. Brown, D. Young, S. Nesic, and M. Singer, in *Corrosion 2018*, p. paper 10984 (2018).
11. S. N. Esmaeely and S. Nesic, *Corrosion*, **eprint**, **early**, DOI: (2019).
12. B. Brown, K.-L. Lee, and S. Nesic, in *Corrosion 2003*, p. paper 03341 (2003).
13. B. F. M. Pots, S. D. Kapusta, R. C. John, M. J. J. S. Thomas, I. J. Rippon, T. S. Whitham, and M. Girgis, in *Corrosion 2002*, p. paper 02235, Denver, Colorado (2002).
14. K.-L. J. Lee and S. Nesic, in *Corrosion 2005*, p. paper 04728 (2005).
15. B. Brown, S. R. Parakala, and S. Nesic, in *Corrosion 2004*, p. paper 04736 (2004).
16. S. N. Smith and J. L. Pacheco, in *Corrosion 2002*, p. Paper 02241, Denver, Colorado (2002).
17. S. N. Smith, *Materials Performance*, **41**, 60 (2002).
18. W. Sun and S. Nesic, *Corrosion 2007*, paper 07655 (2007).
19. J. Sardisco, W. B. Wright, and E. Greco, *Corrosion*, **19**, 354t (1963).
20. E. C. Greco and W. B. Wright, *Corrosion*, **18**, 119t (1962).
21. E. Abelev, T. Ramanarayanan, and S. Bernasek, *Journal of the Electrochemical Society*, **156**, C331 (2009).
22. F. Meyer, O. Riggs, R. McGlasson, and J. Sudbury, *Corrosion*, **14**, 69 (1958).
23. J. Sardisco and R. Pitts, *Corrosion*, **21**, 245 (1965).
24. W. Sun and S. Nešic, *Corrosion*, **65**, 291 (2009).
25. T. J. Edwards, G. Maurer, J. Newman, and J. M. Prausnitz, *AIChe Journal*, **24**, 966 (1978).
26. W. J. DeBruyn, E. Swartz, J. H. Hu, J. A. Shorter, P. Davidovits, D. R. Worsnop, M. S. Zahniser, and C. E. Kolb, *Journal of Geophysical Research-Atmospheres*, **100**, 7245 (1995).
27. M. Ko, B. Ingham, N. Laycock, and D. E. Williams, *Corrosion Science*, **90**, 192 (2015).
28. M. H. Sk, A. M. Abdullah, M. Ko, B. Ingham, N. Laycock, R. Arul, and D. E. Williams, *Corrosion Science*, **126**, 26 (2017).
29. W. Liu, S. L. Lu, Y. Zhang, Z. C. Fang, X. M. Wang, and M. X. Lu, *Materials and Corrosion*, **66**, 1232 (2015).
30. N. Laycock, Effects of Alloy Elements on Corrosion and Hydrogen Permeation in Steels, MSc Dissertation, University of Manchester, Faculty of Technology, 1993.
31. B. Ingham, M. Ko, G. Kear, P. Kappen, N. Laycock, J. A. Kimpton, and D. E. Williams, *Corrosion Science*, **52**, 3052 (2010).
32. B. Ingham, M. Ko, N. Laycock, J. Burnell, P. Kappen, J. A. Kimpton, and D. E. Williams, *Corrosion Science*, **56**, 96 (2012).
33. B. Ingham, M. Ko, N. Laycock, N. M. Kirby, and D. E. Williams, *Faraday Discussions*, **180**, 171 (2015).
34. B. Ingham, M. Ko, P. Shaw, M. H. Sk, A. M. Abdullah, N. Laycock, and D. E. Williams, *Journal of the Electrochemical Society*, **165**, C756 (2018).
35. M. Ko, B. Ingham, N. Laycock, and D. E. Williams, *Corrosion Science*, **80**, 237 (2014).
36. M. Ko, N. J. Laycock, B. Ingham, and D. E. Williams, *Corrosion*, **68**, 1085 (2012).
37. M. H. Sk, A. M. Abdullah, J. Qi, M. Ko, B. Ingham, N. Laycock, M. P. Ryan, and D. E. Williams, *Journal of the Electrochemical Society*, **165**, C278 (2018).
38. M. H. Sk, A. M. Abdullah, M. Ko, N. Laycock, B. Ingham, M. P. Ryan, and D. E. Williams, *ECS Transactions*, **80**, 509 (2017).
39. C. Rodriguez-Navarro, E. Ruiz-Agudo, J. Harris, and S. E. Wolf, *Journal of Structural Biology*, **196**, 260 (2016).
40. R.-Q. Song and H. Cölfen, *CrystEngComm*, **13**, 1249 (2011).
41. M. B. Goldhaber and I. Kaplan, *Marine Chemistry*, **3**, 83 (1975).
42. W. Davison, *Aquatic Sciences*, **53**, 309 (1991).
43. D. C. F. Murcia, P. L. Fosbøl, E. H. Stenby, and K. Thomsen, *Fluid Phase Equilibria*, **475**, 118 (2018).
44. S. Guo, L. Xu, L. Zhang, W. Chang, and M. Lu, *Corrosion Science*, **63**, 246 (2012).
45. B. Wang, L. N. Xu, J. Y. Zhu, H. Xiao, and M. X. Lu, *Corrosion Science*, **111**, 711 (2016).
46. L. N. Xu, B. Wang, J. Y. Zhu, W. Li, and Z. Y. Zheng, *Applied Surface Science*, **379**, 39 (2016).